Physics Letters B 788 (2019) 425–430

Contents lists available at ScienceDirect

Physics Letters B

www.elsevier.com/locate/physletb

Precise QCD description of the Higgs boson transverse momentum spectrum

Xuan Chen [a,*], Thomas Gehrmann [a], E.W. Nigel Glover [b], Alexander Huss [c], Ye Li [d], Duff Neill [e], Markus Schulze [f], Iain W. Stewart [g], Hua Xing Zhu [h]

[a] Department of Physics, University of Zürich, CH-8057 Zürich, Switzerland
[b] Institute for Particle Physics Phenomenology, Department of Physics, University of Durham, Durham, DH1 3LE, UK
[c] Theoretical Physics Department, CERN, CH-1211 Geneva 23, Switzerland
[d] Fermilab, PO Box 500, Batavia, IL 60510, USA
[e] Theoretical Division, MS B283, Los Alamos National Laboratory, Los Alamos, NM 87545, USA
[f] Institut für Physik, Humboldt-Universität zu Berlin, D-12489 Berlin, Germany
[g] Center for Theoretical Physics, Massachusetts Institute of Technology, Cambridge, MA 02139, USA
[h] Department of Physics, Zhejiang University, Hangzhou, 310027, China

ARTICLE INFO

Article history:
Received 17 August 2018
Accepted 19 November 2018
Available online 23 November 2018
Editor: B. Grinstein

Keywords:
Higgs bosons
Perturbative QCD
Resummation
Transverse momentum spectrum

ABSTRACT

The transverse momentum (p_T) distribution of Higgs bosons at hadron colliders enables a detailed probe of its production dynamics and is a key ingredient to precision studies of Higgs boson properties, but receives very large QCD corrections. We obtain a precision prediction for the p_T spectrum by matching second-order (NNLO) QCD corrections at large p_T with resummation of third-order logarithmic (N^3LL) corrections at small p_T. We achieve significantly improved results for $p_T < 35$ GeV with perturbative uncertainties $\lesssim \pm 6\%$, and thus a convergent perturbative series for all values of p_T.

1. Introduction

With the increased statistics and excellent performance of the experiments at the Large Hadron Collider (LHC), precision analysis of the production and decay of the Higgs boson [1–4], the linchpin of the Standard Model, is now becoming reality. Concurrent with the experimental advances has been a concerted effort to improve the theoretical calculations of Higgs production through the gluon fusion mechanism [5–27], driven by the large corrections one finds in the first few orders of perturbation theory. A key observable is the transverse momentum (p_T) spectrum of the Higgs boson with respect to the beam directions, which quantifies how the Higgs boson recoils against partonic radiation, thereby probing the interaction of the Higgs boson with Standard Model particles and possible new states. Calculating the full spectrum requires a combination of fixed order perturbation theory in α_s and a resummation to all orders in α_s of the most singular large logarithms $\ln(p_T/m_H)$ for $p_T \ll m_H$, where m_H is the Higgs mass. In this letter, we compute the transverse momentum spectrum under the infinite top quark mass assumption at the highest precision currently possible, by combining next-to-next-to-leading order (NNLO) at large transverse momentum [20] with an all-order resummation (based on soft-collinear effective field theory, SCET [28–31]) of large logarithmic corrections at small transverse momentum, including subleading logarithms up to the third level (N^3LL) using the recently computed 3-loop rapidity anomalous dimension [32,33]. Our numerical NNLO results extend to considerably smaller values of p_T compared to earlier work [17,20]. Resummation at N^3LL was previously achieved in a momentum space resummation using the `RadISH` Monte Carlo program [26] and matched to NNLO results at low resolution [17]. Our approach to obtain N^3LL resummation uses a SCET factorization formula, which yields analytic expressions for all singular fixed-order terms. Taken together, these two advancements enable a detailed cross-validation of the results from fixed-order and resummation in all parton-level channels, and yield the first high-resolution description of the Higgs boson p_T spectrum.

* Corresponding author.
E-mail address: xuan.chen@uzh.ch (X. Chen).

https://doi.org/10.1016/j.physletb.2018.11.037

2. Method

The dominant Higgs boson production process at the LHC is gluon fusion, mediated by a top quark loop. This process can be described by integrating out the top quark, resulting in an effective field theory (EFT) coupling the Higgs boson to the gluon field strength tensor [34–36], combined with QCD containing five massless quark flavors. The Wilson coefficient of this effective operator is known to three loop accuracy [37], and the validity of this description up to p_T of the order of the top quark mass has been established [22,38] in detail. For higher p_T the exact top quark mass dependence needs to be included, and a recent NLO QCD calculation [23] has demonstrated that this can be accounted for by a multiplicative rescaling of the EFT predictions. The results presented here focus on p_T below the top quark threshold, and are obtained in the EFT framework.

The p_T distribution of the Higgs boson, valid at both small and large p_T, can be written as

$$\frac{d\sigma}{dp_T^2} = \frac{d\sigma^{\rm r}}{dp_T^2} + \left(\frac{d\sigma^{\rm f}}{dp_T^2} - \frac{d\sigma^{\rm s}}{dp_T^2}\right), \tag{1}$$

where $d\sigma^{\rm r}/dp_T^2$ is the resummed distribution, $d\sigma^{\rm f}/dp_T^2$ is the fixed order distribution, and $d\sigma^{\rm s}/dp_T^2$ is the fixed-order singular distribution. The resummed distribution $d\sigma^{\rm r}/dp_T^2$ can be written as an inverse Fourier transformation from impact parameter space $\vec{b}$ to momentum space $\vec{p}_T$, as given in Eq. (2). Here, σ_0 is the Born cross section for $gg \to H$ and we denote $|\vec{b}| = b$ and $b_0 = 2e^{-\gamma_E}$.

$$\begin{aligned}\frac{d\sigma^{\rm r}}{dp_T^2} &= \pi\sigma_0 \int dx_a dx_b \delta\Big(x_a x_b - \frac{m_H^2}{E_{\rm CM}^2}\Big) \\ &\quad\times \int \frac{d^2\vec{b}}{(2\pi)^2} e^{i\vec{p}_T\cdot\vec{b}} W(x_a, x_b, m_H, \vec{b}), \end{aligned}\tag{2}$$

$$\begin{aligned}&W(x_a, x_b, m_H, \vec{b}) \\ &= H(m_H, \mu_h) U_h(m_H, \mu_B, \mu_h) S_\perp(\vec{b}, \mu_s, \nu_s) \\ &\quad\times U_s(b, \mu_B, \mu_s; \nu_B, \nu_s) \\ &\quad\times \prod_{\gamma=a,b} B^{\alpha\beta}_{g/N_\gamma}(x_\gamma, \vec{b}, m_H, \mu_B, \nu_B), \end{aligned}\tag{3}$$

$$\begin{aligned}&U_h(m_H, \mu, \mu_h) \\ &= \exp\left[2\int_{\mu_h}^{\mu} \frac{d\bar\mu}{\bar\mu}\left(\Gamma_{\rm cusp}\big[\alpha_s(\bar\mu)\big]\ln\frac{m_H^2}{\bar\mu^2} + \gamma_V\big[\alpha_s(\bar\mu)\big]\right)\right], \end{aligned}\tag{4}$$

$$\begin{aligned}&U_s(b, \mu, \mu_s; \nu, \nu_s) \\ &= \exp\left[2\int_{\mu_s}^{\mu} \frac{d\bar\mu}{\bar\mu}\left(\Gamma_{\rm cusp}\big[\alpha_s(\bar\mu)\big]\ln\frac{b^2\bar\mu^2}{b_0^2} - \gamma_s\big[\alpha_s(\bar\mu)\big]\right)\right] \\ &\quad\times \left(\frac{\nu^2}{\nu_s^2}\right)^{\int_{\mu}^{b_0/b} \frac{d\bar\mu}{\bar\mu} 2\Gamma_{\rm cusp}[\alpha_s(\bar\mu)] + \gamma_r[\alpha_s(b_0/b)]}, \end{aligned}\tag{5}$$

$$\begin{aligned}&B^{\alpha\beta}_{g/N}(x, \vec{b}, m_H, \mu, \nu) \\ &= \sum_j \int_x^1 \frac{dz}{z} f_{j/N}(x/z, \mu)\left[\frac{g_\perp^{\alpha\beta}}{2} I_{gj}(z, \vec{b}, m_H, \mu, \nu)\right. \\ &\quad\left. + \left(\frac{g_\perp^{\alpha\beta}}{2} + \frac{b^\alpha b^\beta}{b^2}\right) I'_{gj}(z, \vec{b}, m_H, \mu, \nu)\right]. \end{aligned}\tag{6}$$

In Eqs. (2) and (3), the kernel of the integral, W, has been factorized into products of a hard function $H(m_H, \mu_h)$, a soft function $S_\perp(\vec{b}, \mu_s, \nu_s)$, and the beam functions $B^{\alpha\beta}_{g/N_\gamma}(x_\gamma, \vec{b}, m_H, \mu_B, \nu_B)$, each evaluated at an appropriate scale to avoid large logarithms, and subsequently evolved to common scales. Here $f_{j/N}$ are the standard $\overline{\rm MS}$ parton distribution functions and I_{gj} and I'_{gj} are perturbatively calculable matching coefficients. Note that besides the usual renormalization scale μ, the soft function and beam function also depend on the rapidity scale ν. For $p_T \ll m_H$ the resummation is carried out by making the canonical scale choices

$$\mu_h = m_H\,, \quad \mu_B = \mu_s = \nu_s = b_0/b\,, \quad \nu_B = m_H\,, \tag{7}$$

which ensures there are no large logarithms in H, $S_\perp$ and $B^{\alpha\beta}_{g/N_\gamma}$ in Eq. (3). Large logarithms are then resummed through the evolution factors $U_h(m_H, \mu_B, \mu_h)$ and $U_s(b, \mu_B, \mu_s; \nu_B, \nu_s)$, which connect the hard scale and the soft scales to the scales of the beam function, respectively. The U_h and U_s are derived from SCET renormalization group and rapidity renormalization group equations [39,40]. They depend on the cusp anomalous dimension $\Gamma_{\rm cusp}$ [41], the gluon anomalous dimension γ_V [42–44], the soft anomalous dimension γ_s [45,46], and the rapidity anomalous dimension γ_r [33,24], each of which is now known to three loops. In the case of the cusp anomalous dimension, the four-loop leading color approximation is also known [47]. The initial condition of evolution for the hard function and soft function are also known to three-loop order [42–44,46]. In the case of the beam function in Eq. (6), the initial conditions I_{gj} and I'_{gj} are known to two loops [48,49], and the logarithmic terms are known to three loops, which involves the 3-loop splitting functions [41,50]. Our N^{k}LL resummed calculation is obtained from these ingredients, where we include all logarithmic terms at $\mathcal{O}(\alpha_s^k)$ in the H, $S_\perp$ and $B^{\alpha\beta}_{g/N_\gamma}$ boundary conditions. For larger $p_T \sim m_H$ the resummation has to be turned off so that $d\sigma^{\rm r}/dp_T^2 = d\sigma^{\rm s}/dp_T^2$ in Eq. (1) and the cross section reduces to the fixed order result. This is achieved by making a transition of the various μ_i to a single scale, and also transitioning to a single rapidity scale, using profile functions [51,52] as explained below.

The fixed-order (FO) distribution $d\sigma^{\rm f}/dp_T^2$ is obtained as a perturbative expansion in α_s by combining all parton-level contributions that contribute to a given order. As the transverse momentum is fixed to a non-vanishing value, the leading order process is given by the production of the Higgs boson recoiling against a parton. (As a result, the counting of orders (NNLO: $\mathcal{O}(\alpha_s^3)$) is performed with respect to p_T at finite values. For the inclusive Higgs boson production, these would constitute corrections at N^{3}LO.) At higher orders in perturbation theory, a method for the combination of infrared-singular real radiation and virtual loop corrections becomes necessary. In this letter, we employ the antenna subtraction method [53–55] to compute the fixed-order distribution up to NNLO in perturbation theory. The calculation is performed within the parton-level event generator NNLOJET [20], which combines the tree-level double real radiation corrections (RR, [56–58]), the one-loop single real radiation corrections (RV, [59–61]) and the two-loop virtual corrections (VV, [62]) with appropriate antenna subtraction terms. Distributions are obtained as binned histograms in p_T. Schematically, the NNLO contribution to the distribution takes the form

$$\frac{d\sigma_{NNLO}}{dp_T^2} = \int_{\Phi_3}\left[\frac{d\sigma^{RR}_{NNLO}}{dp_T^2} - \frac{d\sigma^{S}_{NNLO}}{dp_T^2}\right]$$

$$+\int_{\Phi_2}\left[\frac{d\sigma^{RV}_{NNLO}}{dp_T^2}-\frac{d\sigma^{T}_{NNLO}}{dp_T^2}\right]$$
$$+\int_{\Phi_1}\left[\frac{d\sigma^{VV}_{NNLO}}{dp_T^2}-\frac{d\sigma^{U}_{NNLO}}{dp_T^2}\right], \tag{8}$$

where the antenna subtraction terms $d\sigma^{S,T,U}_{NNLO}$ (which upon integration add up to zero) ensure the finiteness of each n-parton phase space integral $\int_{\Phi_n}$. Details of the calculation are described in [20], where the transverse momentum distribution was computed to NNLO for large p_T. Extending the lower bound on p_T towards smaller values becomes increasingly challenging due to the large dynamical range probed in the phase-space integration and the associated numerical instabilities. We adapted the NNLOJET code to cope with this task and further split the integration region into several intervals in p_T and applied dedicated reweighting factors in each region. With these optimizations, fixed-order predictions are obtained down to $p_T = 0.7$ GeV, both for a linear binning of 1 GeV width and a logarithmic spacing of ten bins per e-fold.

At small transverse momentum p_T with respect to the Higgs mass m_H, the cross-section can be split into a singular (s) and non-singular (n) piece:

$$\frac{d\sigma^{\rm f}}{dp_T^2}=\frac{d\sigma^{\rm s}}{dp_T^2}+\frac{d\sigma^{\rm n}}{dp_T^2} \tag{9}$$

with

$$\frac{d\sigma^{\rm s}}{dp_T^2}=\frac{\sigma_0}{p_T^2}\sum_{i=1}^{\infty}\left(\frac{\alpha_s}{\pi}\right)^i\sum_{j=0}^{2i-1}c_{i,j}\ln^j\frac{p_T^2}{m_H^2}, \tag{10}$$

$$\frac{d\sigma^{\rm n}}{dp_T^2}=\mathcal{O}\left((p_T/m_H)^0\right). \tag{11}$$

The coefficients $c_{i,j}$ are obtained analytically (up to the integrals over the PDFs) by setting the evolution factors U_h and U_s to unity in Eq. (3), and evaluating the hard function, soft function, and beam function at common scales $\mu_i=\mu_F=\mu_R$ and $\nu_s=\nu_B$. To compare these singular terms with the full fixed order prediction, we integrate Eq. (10) over the same binnings that were used in the numerical evaluation in Eq. (8). Obtaining terms up to the single logarithms in Eq. (10) requires using: NLL at LO, NNLL at NLO and N^{3}LL at NNLO.

For the numerical results, we use the PDF4LHC15NNLO_mc PDFs [63] from the LHAPDF library [64] with its central value of $\alpha_s(m_Z)=0.118$. The center of mass energy of pp collisions is set to 13 TeV. The mass of the Higgs boson and top quark (dependence in the Wilson coefficient) are set to be $m_H=125$ GeV and $m_t=173.2$ GeV. The central values for the factorization and renormalization scales are chosen as $\mu_F=\mu_R=m_H/2$, with the theory error from fixed order calculations estimated from the envelope of a three-point variation between $m_H/4$ and m_H.

Fig. 1 compares the fixed-order contributions at LO, NLO and NNLO for the transverse momentum spectrum where the curve labeled as the SCET prediction is $p_T d\sigma^{\rm s}/dp_T = 2p_T^2\, d\sigma^{\rm s}/dp_T^2$ at the corresponding order. For better visibility, the distributions are multiplied by p_T, and each higher order contribution is displayed separately, instead of being added to the previous orders. The bottom panels show the difference of the two curves, i.e. the non-singular parts which should behave as $p_T d\sigma^{\rm n}/dp_T \sim \mathcal{O}(p_T^2)$ for $p_T \ll m_H$, to further elucidate the low-p_T behavior between the two predictions. The top frame shows that the small p_T behavior of the fixed-order spectrum is in excellent agreement with the

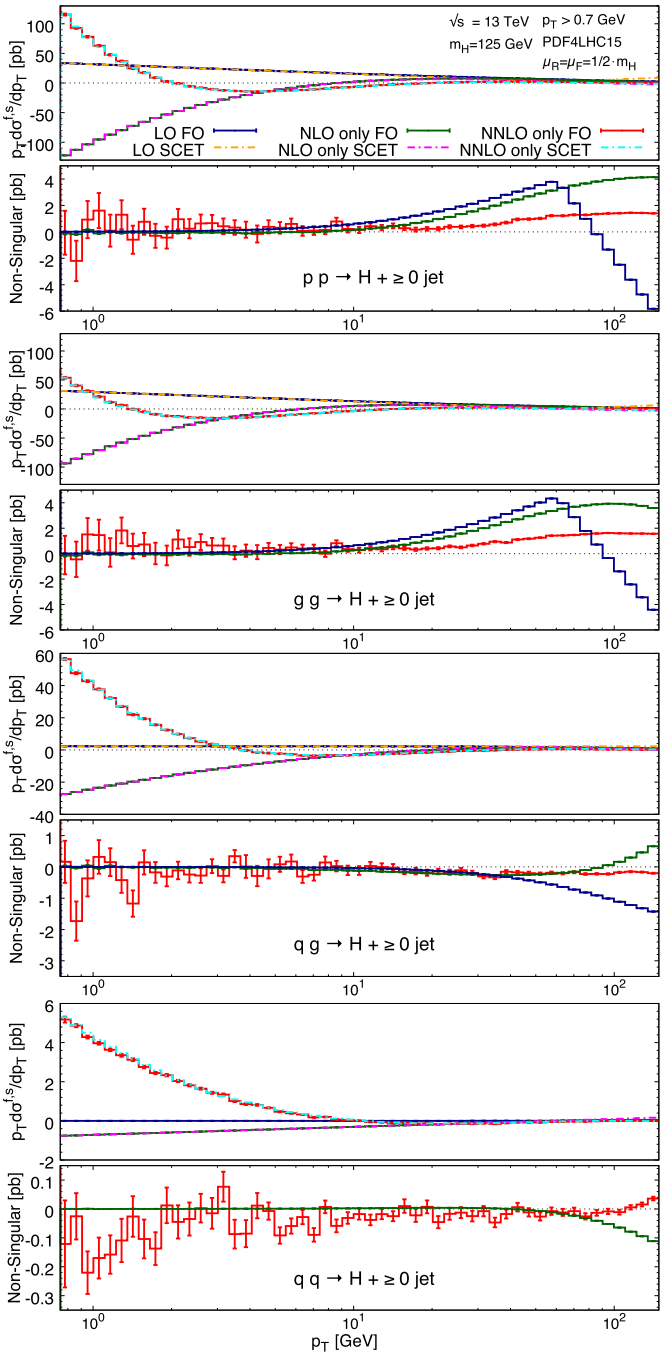

Fig. 1. Comparison of the transverse momentum spectrum between fixed-order perturbation theory (FO) and singular terms from the expansion of the resummed prediction (SCET), using the sum of all partonic channels (pp) or with individual partonic channels (gg, qg, qq). In individual channels, q denotes the sum of quark and anti-quark of all flavors.

predicted singular terms in Eq. (10). This agreement is further substantiated in the lower three frames, where individual parton-level initial states are compared (with q denoting the sum over quarks and antiquarks of all light flavors). We point out that the (numerically subdominant) qq channel turns out to be the numerically most challenging, since contributions from valence-valence scattering favor events with higher partonic center-of-mass energy than in any of the other channels. The excellent agreement between fixed-order perturbation theory and SCET-predictions for the singular terms serves as a very strong mutual cross check of both ap-

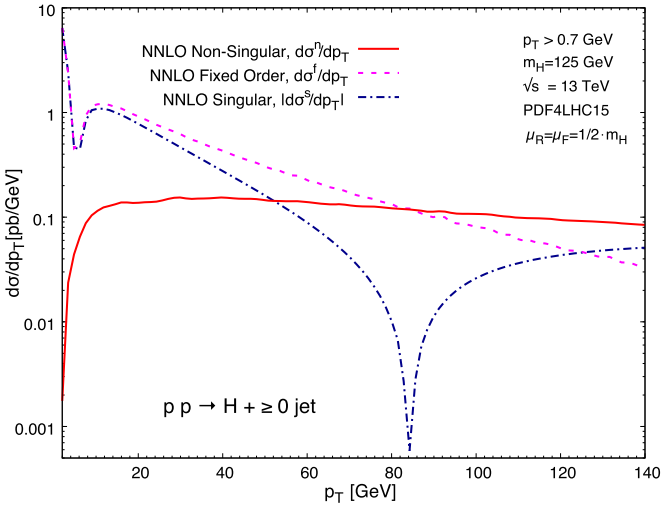

Fig. 2. Comparison of full fixed-order spectrum, the absolute value of singular distribution, and the non-singular distribution through to NNLO. Here $d\sigma^{n}/dp_T \sim \mathcal{O}(p_T)$ for $p_T \ll m_H$.

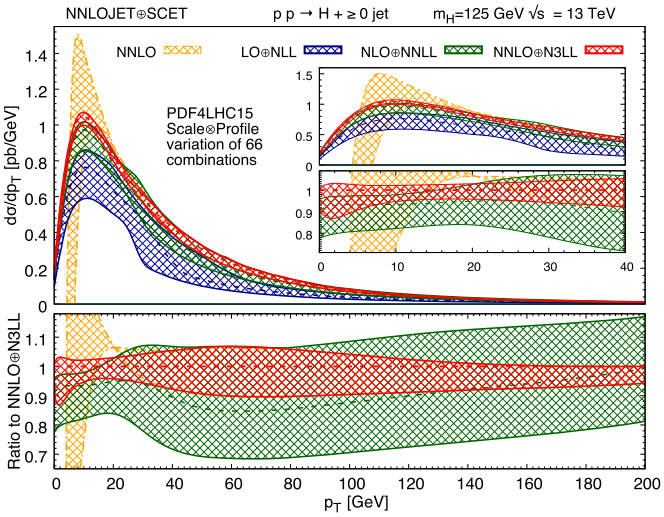

Fig. 3. The Higgs-boson transverse momentum distribution matched between FO and SCET. Dashed lines indicate central scales of $m_H/2$ and matching profile centered at 30 GeV. The theoretical uncertainties are estimated by taking the envelope of all scale and profile variations (see text). Ratio plots in the lower panel presents the scale and profile variation with respect to the central result for NNLO + N^3LL (red dashed line).

proaches. It demonstrates that our calculation of the non-singular terms is reliable over a broad range in p_T, thereby enabling a consistent matching of the NNLO and N^3LL predictions.

3. Matching and results

For a reliable description of the transverse-momentum spectrum, the resummation of large logarithms in $d\sigma^{s}/dp_T^2$ has to be turned off at large p_T. This can be seen clearly from Fig. 2, which depicts the full fixed-order spectrum, the absolute value of singular distribution, and the non-singular distribution, all through to NNLO. At $p_T \ll 50$ GeV, the singular distribution dominates the fixed-order cross section, and the resummation of higher order logarithms is necessary. Around 50 GeV, the singular and non-singular distribution become comparable, and resummation has to be gradually turned off. The NNLO singular pieces turn negative and largely constant above $p_T \approx 85$ GeV, indicating that the decomposition of the NNLO fixed order prediction into singular and non-singular pieces is losing its meaning there. There are several different prescriptions on how to turn off the resummation [65–67, 12,68,16,69,26]. In this letter, we follow Ref. [16] by introducing b and p_T dependent profile functions, defining

$$\rho(b,p_T) = \frac{\rho_l}{2}\Big[1-\tanh\Big(4s\Big(\frac{p_T}{t}-1\Big)\Big)\Big] + \frac{\rho_r}{2}\Big[1+\tanh\Big(4s\Big(\frac{p_T}{t}-1\Big)\Big)\Big], \tag{12}$$

where $\rho(b,p_T)$ is used for $\mu_s = \mu_s(b,p_T) = \mu_B$, $\nu_s = \nu_s(b,p_T)$, and $\mu_h = \mu_h(p_T)$, which appear in Eq. (3). ρ_l is the initial scale for each profile, taken to be the canonical scales in Eq. (7) so that at small p_T the large logarithms are resummed. ρ_r is the final scale for each profile, which is chosen to be $\mu_h = \mu_B = \mu_s = \mu_F = \mu_R$, while for ν_s it is m_H. The parameters s and t govern the rate of transition between the fixed order result and the resummation, where the transition starts at $p_T \simeq t - t/(2s)$, is centered at $p_T = t$, and ends at $p_T \simeq t + t/(2s)$. In our calculation, we choose $s = 1$, and $t = 20, 25, 30, 35, 40, 50$ GeV to estimate the uncertainties from different profiles. The uncertainties for the final resummed + fixed-order prediction are estimated by three-point variations of i) the ρ_l for μ_h about m_H and ρ_r for all scales (varied simultaneously), and ii) the ρ_l for $\mu_B = \mu_s$ and ν_s about b_0/b (varied independently). We always fix $\nu_B = m_H$. We take the envelope of the resulting 66 curves as the uncertainty band at each order. Further uncertainties in our calculation include the missing four-loop cusp anomalous dimension and the treatment of non-perturbative corrections at large b. They are estimated to be negligible compared with the aforementioned scale uncertainties. Additional independent uncertainties related to the parton distributions and value of $\alpha_s(m_Z)$ should be included for a detailed phenomenological study.

The final matched transverse momentum spectrum is shown in Fig. 3. We plot the distributions at LO + NLL, NLO + NNLL, and NNLO + N^3LL. We also plot the unmatched NNLO distribution. At small transverse momentum, the fixed order distribution displays unphysical behavior, due to the presence of large logarithms. We see that the matched distribution smoothly merges into the fixed-order cross section around 40 GeV, and that the scale uncertainty reduces order-by-order in perturbation theory. The perturbative uncertainties at NNLO + N^3LL have been reduced to $\lesssim \pm 6\%$ for $5 < p_T < 35$ GeV, are $\pm 10\%$ for intermediate p_T, and decreasing again at large p_T.

4. Conclusions

In this letter we have presented for the first time precise predictions for the Higgs transverse momentum spectrum at small p_T, with resummation at N^3LL matched to fixed-order results at NNLO. The calculation builds upon efficient subtraction formalism for jet processes, improved formalism for resummation of large transverse logarithms, and known high-order anomalous dimensions and matching coefficients. We use an additive matching scheme which relies on the extraction of non-singular corrections from singular ones, and usually requires numerical Monte Carlo precision at the level of 1 per-mille, which imposes a strong challenge on fixed-order calculations in the infrared unstable small p_T region. We have shown excellent agreement between SCET and NNLOJET in this region, which provides a highly nontrivial check of both calculations. The final matched predictions show a continuous reduction of scale uncertainties order by order, and are significantly more precise for small p_T. We expect our results will have an important impact on understanding the detailed properties of the Higgs boson at the LHC.

Acknowledgements

We thank the University of Zurich S3IT and CSCS Lugano for providing the computational resources for this project. This research was supported in part by the UK Science and Technology Facilities Council under contract ST/G000905/1, by the Swiss National Science Foundation (SNF) under contracts 200020-175595 and CRSII2-160814, by the Swiss National Supercomputing Centre (CSCS) under project ID UZH10, by the Research Executive Agency (REA) of the European Union under the ERC Advanced Grant MC@NNLO (340983), Department of Energy under Contracts No. DE-SC0011090 and DE-AC52-06NA25396, by the Simons Foundation Investigator Grant No. 327942, by the LANL/LDRD Program, within the framework of the TMD Topical Collaboration, and by a startup grant from Zhejiang University.

References

[1] S. Chatrchyan, et al., Observation of a new boson at a mass of 125 GeV with the CMS experiment at the LHC, Phys. Lett. B 716 (2012) 30–61, arXiv:1207.7235.
[2] G. Aad, et al., Observation of a new particle in the search for the Standard Model Higgs boson with the ATLAS detector at the LHC, Phys. Lett. B 716 (2012) 1–29, arXiv:1207.7214.
[3] G. Aad, et al., Measurements of fiducial and differential cross sections for Higgs boson production in the diphoton decay channel at $\sqrt{s} = 8$ TeV with ATLAS, J. High Energy Phys. 09 (2014) 112, arXiv:1407.4222.
[4] V. Khachatryan, et al., Measurement of differential cross sections for Higgs boson production in the diphoton decay channel in pp collisions at $\sqrt{s} = 8$ TeV, Eur. Phys. J. C 76 (1) (2016) 13, arXiv:1508.07819.
[5] D. de Florian, M. Grazzini, Z. Kunszt, Higgs production with large transverse momentum in hadronic collisions at next-to-leading order, Phys. Rev. Lett. 82 (1999) 5209–5212, arXiv:hep-ph/9902483.
[6] R.V. Harlander, W.B. Kilgore, Next-to-next-to-leading order Higgs production at hadron colliders, Phys. Rev. Lett. 88 (2002) 201801, arXiv:hep-ph/0201206.
[7] C. Anastasiou, K. Melnikov, Higgs boson production at hadron colliders in NNLO QCD, Nucl. Phys. B 646 (2002) 220–256, arXiv:hep-ph/0207004.
[8] V. Ravindran, J. Smith, W.L. van Neerven, NNLO corrections to the total cross-section for Higgs boson production in hadron–hadron collisions, Nucl. Phys. B 665 (2003) 325–366, arXiv:hep-ph/0302135.
[9] V. Ravindran, J. Smith, W.L. Van Neerven, Next-to-leading order QCD corrections to differential distributions of Higgs boson production in hadron–hadron collisions, Nucl. Phys. B 634 (2002) 247–290, arXiv:hep-ph/0201114.
[10] C. Anastasiou, C. Duhr, F. Dulat, F. Herzog, B. Mistlberger, Higgs boson gluon-fusion production in QCD at three loops, Phys. Rev. Lett. 114 (2015) 212001, arXiv:1503.06056.
[11] B. Mistlberger, Higgs boson production at hadron colliders at N^3LO in QCD, J. High Energy Phys. 05 (2018) 028, arXiv:1802.00833.
[12] G. Bozzi, S. Catani, D. de Florian, M. Grazzini, Transverse-momentum resummation and the spectrum of the Higgs boson at the LHC, Nucl. Phys. B 737 (2006) 73–120, arXiv:hep-ph/0508068.
[13] S. Mantry, F. Petriello, Factorization and resummation of Higgs boson differential distributions in soft-collinear effective theory, Phys. Rev. D 81 (2010) 093007, arXiv:0911.4135.
[14] D. de Florian, G. Ferrera, M. Grazzini, D. Tommasini, Transverse-momentum resummation: Higgs boson production at the Tevatron and the LHC, J. High Energy Phys. 11 (2011) 064, arXiv:1109.2109.
[15] T. Becher, M. Neubert, D. Wilhelm, Higgs-boson production at small transverse momentum, J. High Energy Phys. 05 (2013) 110, arXiv:1212.2621.
[16] D. Neill, I.Z. Rothstein, V. Vaidya, The Higgs transverse momentum distribution at NNLL and its theoretical errors, J. High Energy Phys. 12 (2015) 097, arXiv:1503.00005.
[17] R. Boughezal, F. Caola, K. Melnikov, F. Petriello, M. Schulze, Higgs boson production in association with a jet at next-to-next-to-leading order, Phys. Rev. Lett. 115 (8) (2015) 082003, arXiv:1504.07922.
[18] R. Boughezal, C. Focke, W. Giele, X. Liu, F. Petriello, Higgs boson production in association with a jet at NNLO using jettiness subtraction, Phys. Lett. B 748 (2015) 5–8, arXiv:1505.03893.
[19] F. Caola, K. Melnikov, M. Schulze, Fiducial cross sections for Higgs boson production in association with a jet at next-to-next-to-leading order in QCD, Phys. Rev. D 92 (7) (2015) 074032, arXiv:1508.02684.
[20] X. Chen, J. Cruz-Martinez, T. Gehrmann, E.W.N. Glover, M. Jaquier, NNLO QCD corrections to Higgs boson production at large transverse momentum, J. High Energy Phys. 10 (2016) 066, arXiv:1607.08817.
[21] F. Caola, S. Forte, S. Marzani, C. Muselli, G. Vita, The Higgs transverse momentum spectrum with finite quark masses beyond leading order, J. High Energy Phys. 08 (2016) 150, arXiv:1606.04100.
[22] R. Frederix, S. Frixione, E. Vryonidou, M. Wiesemann, Heavy-quark mass effects in Higgs plus jets production, J. High Energy Phys. 08 (2016) 006, arXiv:1604.03017.
[23] S.P. Jones, M. Kerner, G. Luisoni, NLO QCD corrections to Higgs boson plus jet production with full top-quark mass dependence, Phys. Rev. Lett. 120 (16) (2018) 162001, arXiv:1802.00349.
[24] A.A. Vladimirov, Correspondence between soft and rapidity anomalous dimensions, Phys. Rev. Lett. 118 (6) (2017) 062001, arXiv:1610.05791.
[25] P.F. Monni, E. Re, P. Torrielli, Higgs transverse-momentum resummation in direct space, Phys. Rev. Lett. 116 (24) (2016) 242001, arXiv:1604.02191.
[26] W. Bizon, P.F. Monni, E. Re, L. Rottoli, P. Torrielli, Momentum-space resummation for transverse observables and the Higgs $p_\perp$ at $N^3LL + NNLO$, J. High Energy Phys. 02 (2018) 108, arXiv:1705.09127.
[27] F. Caola, J.M. Lindert, K. Melnikov, P.F. Monni, L. Tancredi, C. Wever, Bottom-quark effects in Higgs production at intermediate transverse momentum, J. High Energy Phys. 09 (2018) 035, arXiv:1804.07632.
[28] C.W. Bauer, S. Fleming, M.E. Luke, Summing Sudakov logarithms in $B \to X_s + \gamma$ in effective field theory, Phys. Rev. D 63 (2000) 014006, arXiv:hep-ph/0005275.
[29] C.W. Bauer, S. Fleming, D. Pirjol, I.W. Stewart, An effective field theory for collinear and soft gluons: heavy to light decays, Phys. Rev. D 63 (2001) 114020, arXiv:hep-ph/0011336.
[30] C.W. Bauer, D. Pirjol, I.W. Stewart, Soft collinear factorization in effective field theory, Phys. Rev. D 65 (2002) 054022, arXiv:hep-ph/0109045.
[31] C.W. Bauer, S. Fleming, D. Pirjol, I.Z. Rothstein, I.W. Stewart, Hard scattering factorization from effective field theory, Phys. Rev. D 66 (2002) 014017, arXiv:hep-ph/0202088.
[32] Y. Li, D. Neill, H.X. Zhu, An exponential regulator for rapidity divergences, arXiv:1604.00392.
[33] Y. Li, H.X. Zhu, Bootstrapping rapidity anomalous dimensions for transverse-momentum resummation, Phys. Rev. Lett. 118 (2) (2017) 022004, arXiv:1604.01404.
[34] F. Wilczek, Decays of heavy vector mesons into Higgs particles, Phys. Rev. Lett. 39 (1977) 1304.
[35] M.A. Shifman, A.I. Vainshtein, V.I. Zakharov, Remarks on Higgs boson interactions with nucleons, Phys. Lett. B 78 (1978) 443–446.
[36] T. Inami, T. Kubota, Y. Okada, Effective gauge theory and the effect of heavy quarks in Higgs boson decays, Z. Phys. C 18 (1983) 69.
[37] K.G. Chetyrkin, B.A. Kniehl, M. Steinhauser, Decoupling relations to $\mathcal{O}(\alpha_s^3)$ and their connection to low-energy theorems, Nucl. Phys. B 510 (1998) 61–87, arXiv:hep-ph/9708255.
[38] T. Neumann, C. Williams, The Higgs boson at high p_T, Phys. Rev. D 95 (1) (2017) 014004, arXiv:1609.00367.
[39] J.-y. Chiu, A. Jain, D. Neill, I.Z. Rothstein, The rapidity renormalization group, Phys. Rev. Lett. 108 (2012) 151601, arXiv:1104.0881.
[40] J.-Y. Chiu, A. Jain, D. Neill, I.Z. Rothstein, A formalism for the systematic treatment of rapidity logarithms in quantum field theory, J. High Energy Phys. 05 (2012) 084, arXiv:1202.0814.
[41] S. Moch, J.A.M. Vermaseren, A. Vogt, The three loop splitting functions in QCD: the nonsinglet case, Nucl. Phys. B 688 (2004) 101–134, arXiv:hep-ph/0403192.
[42] P.A. Baikov, K.G. Chetyrkin, A.V. Smirnov, V.A. Smirnov, M. Steinhauser, Quark and gluon form factors to three loops, Phys. Rev. Lett. 102 (2009) 212002, arXiv:0902.3519.
[43] R.N. Lee, A.V. Smirnov, V.A. Smirnov, Analytic results for massless three-loop form factors, J. High Energy Phys. 04 (2010) 020, arXiv:1001.2887.
[44] T. Gehrmann, E.W.N. Glover, T. Huber, N. Ikizlerli, C. Studerus, Calculation of the quark and gluon form factors to three loops in QCD, J. High Energy Phys. 06 (2010) 094, arXiv:1004.3653.
[45] T. Becher, M. Neubert, G. Xu, Dynamical threshold enhancement and resummation in Drell–Yan production, J. High Energy Phys. 07 (2008) 030, arXiv:0710.0680.
[46] Y. Li, A. von Manteuffel, R.M. Schabinger, H.X. Zhu, Soft-virtual corrections to Higgs production at N^3LO, Phys. Rev. D 91 (2015) 036008, arXiv:1412.2771.
[47] S. Moch, B. Ruijl, T. Ueda, J.A.M. Vermaseren, A. Vogt, Four-loop non-singlet splitting functions in the planar limit and beyond, J. High Energy Phys. 10 (2017) 041, arXiv:1707.08315.
[48] T. Gehrmann, T. Lübbert, L.L. Yang, Calculation of the transverse parton distribution functions at next-to-next-to-leading order, J. High Energy Phys. 06 (2014) 155, arXiv:1403.6451.
[49] M.G. Echevarria, I. Scimemi, A. Vladimirov, Unpolarized transverse momentum dependent parton distribution and fragmentation functions at next-to-next-to-leading order, J. High Energy Phys. 09 (2016) 004, arXiv:1604.07869.
[50] A. Vogt, S. Moch, J.A.M. Vermaseren, The three-loop splitting functions in QCD: the singlet case, Nucl. Phys. B 691 (2004) 129–181, arXiv:hep-ph/0404111.
[51] Z. Ligeti, I.W. Stewart, F.J. Tackmann, Treating the b quark distribution function with reliable uncertainties, Phys. Rev. D 78 (2008) 114014, arXiv:0807.1926.
[52] R. Abbate, M. Fickinger, A.H. Hoang, V. Mateu, I.W. Stewart, Thrust at N^3LL with power corrections and a precision global fit for $\alpha_s(m_Z)$, Phys. Rev. D 83 (2011) 074021, arXiv:1006.3080.

[53] A. Gehrmann-De Ridder, T. Gehrmann, E.W.N. Glover, Quark-gluon antenna functions from neutralino decay, Phys. Lett. B 612 (2005) 36–48, arXiv:hep-ph/0501291.

[54] A. Daleo, T. Gehrmann, D. Maitre, Antenna subtraction with hadronic initial states, J. High Energy Phys. 04 (2007) 016, arXiv:hep-ph/0612257.

[55] J. Currie, E.W.N. Glover, S. Wells, Infrared structure at NNLO using antenna subtraction, J. High Energy Phys. 04 (2013) 066, arXiv:1301.4693.

[56] V. Del Duca, A. Frizzo, F. Maltoni, Higgs boson production in association with three jets, J. High Energy Phys. 05 (2004) 064, arXiv:hep-ph/0404013.

[57] L.J. Dixon, E.W.N. Glover, V.V. Khoze, MHV rules for Higgs plus multi-gluon amplitudes, J. High Energy Phys. 12 (2004) 015, arXiv:hep-th/0411092.

[58] S.D. Badger, E.W.N. Glover, V.V. Khoze, MHV rules for Higgs plus multi-parton amplitudes, J. High Energy Phys. 03 (2005) 023, arXiv:hep-th/0412275.

[59] L.J. Dixon, Y. Sofianatos, Analytic one-loop amplitudes for a Higgs boson plus four partons, J. High Energy Phys. 08 (2009) 058, arXiv:0906.0008.

[60] S. Badger, E.W.N. Glover, P. Mastrolia, C. Williams, One-loop Higgs plus four gluon amplitudes: full analytic results, J. High Energy Phys. 01 (2010) 036, arXiv:0909.4475.

[61] S. Badger, J.M. Campbell, R.K. Ellis, C. Williams, Analytic results for the one-loop NMHV Hqqgg amplitude, J. High Energy Phys. 12 (2009) 035, arXiv:0910.4481.

[62] T. Gehrmann, M. Jaquier, E.W.N. Glover, A. Koukoutsakis, Two-loop QCD corrections to the helicity amplitudes for $H \to 3$ partons, J. High Energy Phys. 02 (2012) 056, arXiv:1112.3554.

[63] J. Butterworth, et al., PDF4LHC recommendations for LHC Run II, J. Phys. G 43 (2016) 023001, arXiv:1510.03865.

[64] A. Buckley, J. Ferrando, S. Lloyd, K. Nordström, B. Page, M. Rüfenacht, M. Schönherr, G. Watt, LHAPDF6: parton density access in the LHC precision era, Eur. Phys. J. C 75 (2015) 132, arXiv:1412.7420.

[65] J.C. Collins, D.E. Soper, G.F. Sterman, Transverse momentum distribution in Drell–Yan pair and W and Z boson production, Nucl. Phys. B 250 (1985) 199–224.

[66] P.B. Arnold, R.P. Kauffman, W and Z production at next-to-leading order: from large $q(t)$ to small, Nucl. Phys. B 349 (1991) 381–413.

[67] C. Balazs, C.P. Yuan, Soft gluon effects on lepton pairs at hadron colliders, Phys. Rev. D 56 (1997) 5558–5583, arXiv:hep-ph/9704258.

[68] D. Boer, W.J. den Dunnen, TMD evolution and the Higgs transverse momentum distribution, Nucl. Phys. B 886 (2014) 421–435, arXiv:1404.6753.

[69] J. Collins, L. Gamberg, A. Prokudin, T.C. Rogers, N. Sato, B. Wang, Relating transverse momentum dependent and collinear factorization theorems in a generalized formalism, Phys. Rev. D 94 (3) (2016) 034014, arXiv:1605.00671.